Journal of Alloys and Compounds 520 (2012) 255–261

Contents lists available at SciVerse ScienceDirect

Journal of Alloys and Compounds

journal homepage: www.elsevier.com/locate/jallcom

Physical properties of polycrystalline Dy_2PdGe_6 and La_2PdGe_6

R. Wawryk[a,*], R. Troć[a], A.V. Gribanov[b]

[a] W. Trzebiatowski Institute of Low Temperature and Structure Research Polish Academy of Sciences, 50-950 Wrocław 2, P.O. Box 1410, Poland
[b] Chemistry Department of the Moscow State University, Leninskie Gory, GSP-3, 119899 Moscow, Russia

ARTICLE INFO

Article history:
Received 25 November 2011
Received in revised form 4 January 2012
Accepted 5 January 2012
Available online 14 January 2012

Keywords:
Rare earth compound
Magnetic properties
Electrical transport
Specific heat
Thermoelectric power

ABSTRACT

Polycrystalline samples of the intermetallic compounds Dy_2PdGe_6 and La_2PdGe_6 which crystallize in the orthorhombic structure (*Cmca* space group) were studied by means of magnetic, electrical resistivity, specific heat and differential thermoelectric power measurements. The Dy-germanide is an antiferromagnet below 25(1) K and at low temperature and above magnetic fields of 3.5 T it exhibits a metamagnetic behaviour. Especially the specific heat measurements point to well-localized 4*f*-electrons in this compound. Whereas the isostructural La-germanide is a nonmagnetic material taken here as a reference compound. A good overall fit of the resistivity to a general Bloch–Grüneisen formula indicates its metallic character in contrast to the Dy-germanide being a semimetallic-like conductor. For the latter compound in its ordered state the electrical resistvity, specific heat and thermoelectric power are dominated by electron–magnon scattering with antiferromagnetic spin-wave spectrum typical of anisotropic antiferromagnetic systems. The observed Schottky anomaly yields an assumed crystal field scheme of low-energy lying levels. Its thermoelectric power behaviour achieves medium positive values at high temperatures, indicating a hole domination in electrical transport properties. On the other hand, $S(T)$ below T_N for Dy- and in the whole temperatures measured for La-based compounds is negative, pointing to their electron carrier origin.

1. Introduction

More than two decades ago some novel ternary compounds with general chemical formula R_2TGe_6, where R is a rare earth element and T is a transition metal as Pd, Pt, Cu, Ag, Au, were synthesized [1] and found to crystallize in the orthorhombic structure of the Ce_2CuGe_6 type (*Amm2* space group) [2]. However, in 2002 the new atomic order for one compound from this family, namely Yb_2PdGe_6, was reported by Fornasini et al. [3], which differs from that in the Ce_2CuGe_6 type. Contrary to the prior reports, we have established in the present work from the X-ray powder diffraction experiment that the crystal structures of both La_2TGe_6 and Dy_2TGe_6 also belong to this new Yb_2PdGe_6-type (*Cmca* space group).

The R_2CuGe_6 compounds with both a light (R = Ce, Pr, Nd, and Sm) and heavy (R = Gd, Tb, Dy, and Er) rare elements, all exhibit an antiferromagnetic ordering below around 20 K [4,5]. Contrary to all of them, Yb_2CuGe_6 displays a mixed-valence character of 4*f*-electrons [6,7]. Recently, the magnetic properties of another series of such germanides with the same stoichiometry, namely R_2NiGe_6 (R = Gd, Dy, Ho), have also been reported to be antiferromagnets [8,9]. As expected, such ternary germanides based on Y with T = Cu and Ni behave as Pauli-like paramagnets [4,9]. It was found that for heavy rare-earth representatives for both containing Cu and Ni, their Néel temperatures T_N's are proportional to the de Gennes factor $(g_J - 1)^2 J(J+1)$ [5,9]. Moreover, the effective magnetic moments of the R ions agree well with the values of theoretical tripositive ions. Some data for the transport properties of a series of R_2TGe_6 compounds with T = Mn, Ni and Cu, measured on polycrystalline samples, have also been reported [10].

Up to now only a few such germanides have been studied containing Pd or Pt. They are Ce_2(Pd: Pt)Ge_6 [11,12,1] as well as Sm_2(Pd,Pt)Ge_6 [13]. In the present paper, we provide the results of our detailed measurements of magnetization, magnetic susceptibility, electrical resistivity, thermoelectric power, and thermal properties made for polycrystalline Dy_2PdGe_6 and its reference compound La_2PdGe_2. All results obtained indicate that this Dy-based compound orders antiferromagnetically, and its temperature dependence of the specific heat and the thermoelectric power are characteristic of an anisotropic antiferromagnet due to the presence of magnetocrystalline anisotropy. In this compound the magnetic properties are established by stable Dy $4f^9$-electrons being well localized and strongly influenced by crystal-electric-field (CEF) effect already at the medium range of temperatures.

2. Experimental details

The polycrystalline samples of Dy_2PdGe_6 and La_2PdGe_6 were prepared by arc melting stoichiometric amounts of the elements: Dy (or La), Pd and Ge, under pure argon atmosphere, using a non-consumable tungsten electrode and a cold copper

* Corresponding author.
E-mail address: R.Wawryk@int.pan.wroc.pl (R. Wawryk).

0925-8388/$ – see front matter © 2012 Elsevier B.V. All rights reserved.
doi:10.1016/j.jallcom.2012.01.036

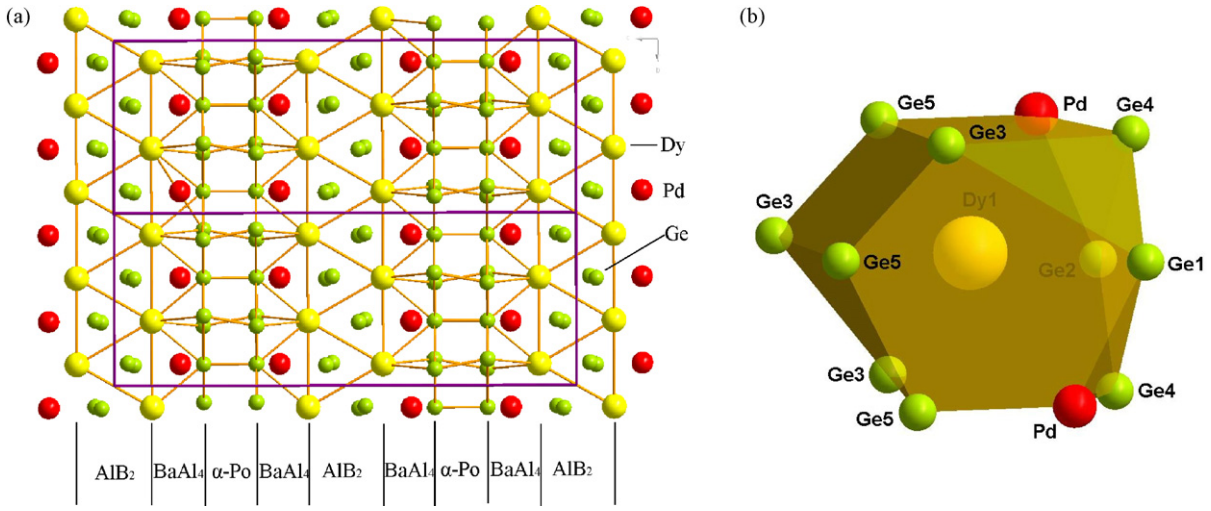

Fig. 1. (a) Sketch of the orthorhombic crystal structure of $(La,Dy)_2PdGe_6$. (b) Coordination polyhedron around Dy central atom.

hearth. High purity starting elements were used: Dy (or La) at least with 99.8 wt.%, Pd with 99.95 wt.%, and Ge with 99.999 wt.%. The weight loses of as-cast ingots was about 0.5 wt.%. To ensure homogenisation, all alloys were re-melted three times. Such obtained samples were then vacuum-sealed in a quartz tube and annealed at 700 °C for 15 days before being quenched into cold water. X-ray powder diffraction patterns from annealed alloys were collected with "STOE STADIP" equipment (Cu Kα; $7° < 2\theta < 100°$, step 0.1°). Lattice parameters were calculated using the STOE-WinXpow software.

A Quantum Designed (QD) SQUID magnetometer was used for magnetization measurements in fields up to 5 Tesla at a temperature of 2 K. The susceptibility was measured over the range $1.7 \le T \le 400$ K. The electrical resistivity was examined between 0.35 and 300 K using two homemade experimental set-ups and four-lead AC method. Spark cutting was used to form an elongated specimen for measurements. The samples dimensions were of about 4 mm × 1 mm × 1 mm. The contact places were first electrochemically covered by a thin layer of copper, and then silver leads were attached to the sample by a silver paste.

Thermoelectric power was measured on a sample presenting two polished faces from 6 to 300 K in a homemade set-up using a differential method. The pure copper was used as a reference material. The low temperature behaviour (between 0.35 and 6 K) was obtained using another homemade setup. The temperature dependence of the specific heat between 2 and 300 K was measured by relaxation method with a commercial QD PPMS-9 apparatus.

3. Results and discussion

3.1. Crystal structure and magnetic properties

The X-ray diagrams obtained at room temperature (RT) by using monochromatic Cu Kα radiation have shown that both La- and Dy-palladium-germanide samples were almost single phases. One could detect the presence of unknown impurities amounting up to 3.5%. The least squares calculated values of the lattice parameters are given in Table 1.

In the unit cell of the Yb_2CuGe_6-type (*s.g. Cmca*, No. 64, Z = 2) the atoms occupy the following positions: Dy and Ge1 atoms at the 16 g sites: [x, y, z_i], Pd atoms as well as Ge3, Ge4, Ge5, atoms at the 2a site: [0, y_i, z_i] with different y_i and z_i for each corresponding atoms. They are similar to those given in Ref. [3] for the case of Yb-based compound. Figure presenting the sketch of the orthorhombic crystal structure (for the two cells) of the studied compounds is given in Fig. 1(a). It can be described as the sequence of atomic planes stacked along the much-elongated *c*-axis with very close values of the *a* and *b* axes ($c/a(b) \approx 2.63(2.68)$) (for both La- and Dy-based unit cells) and forming a layered structure giving rise to fairly large distances between the magnetic atoms along the *c*-axis.

This structure can be also described as a sequence of the following slabs of the AlB_2-, $BaAl_4$- and αPo-type along the *c*-direction [3]. In the AlB_2 fragment, the Dy-trigonal prism (yellow balls) are centered by the Ge atoms. The d_{Dy-Dy} distances are equal to 0.396 nm. Thus for better understanding the two cells projected on *yz* plane is shown in Fig. 1(a). The Dy atom is surrounded by two Pd atoms and 9 germanium atoms (CN = 11), forming irregular geometric figure (see Fig. 1(b)).

In Fig. 2 the reciprocal magnetic susceptibility $\chi^{-1}(T)$ is plotted against the temperature. The low temperature susceptibility variation $\chi(T)$, in the form of a λ-type cusp, given in the upper inset of this figure, indicates an antiferromagnetic (AFM) transition with the Néel temperature (T_N) of 25(1) K. As seen from Fig. 2, the $\chi^{-1}(T)$ dependence is well followed by the Curie–Weiss law above

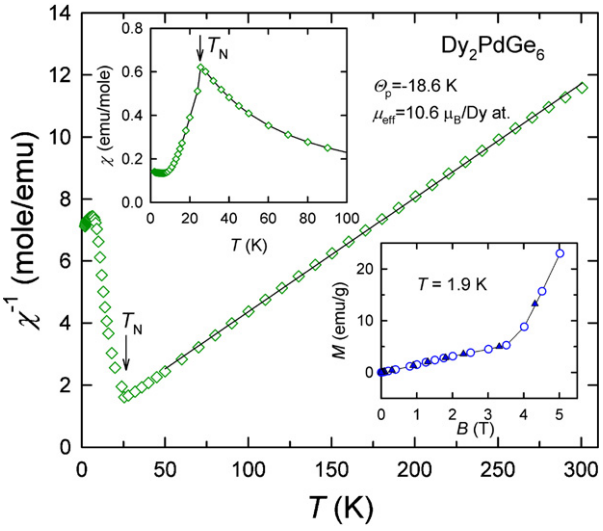

Fig. 2. Reciprocal magnetic susceptibility vs. temperature of the polycrystalline Dy_2PdGe_6 sample. The solid line denotes the linear fit of the $\chi^{-1}(T)$ function to the Curie–Weiss law. The upper inset presents the susceptibility behaviour at low-*T*, whilst the lower inset shows the magnetization vs. magnetic field measured at 1.9 K. The magnetization was measured in increasing (open circles) and decreasing (solid triangles) fields.

Table 1
Lattice parameters of $(La:Dy)_2PdGe_6$ (in nm units).

Compound	*a*	*b*	*c*	*V* (nm^3)
La_2PdGe_6	0.84301(10)	0.82180(7)	2.2192(3)	1.5374(4)
Dy_2PdGe_6	0.81361(3)	0.80202(3)	2.1447(1)	1.3995(1)

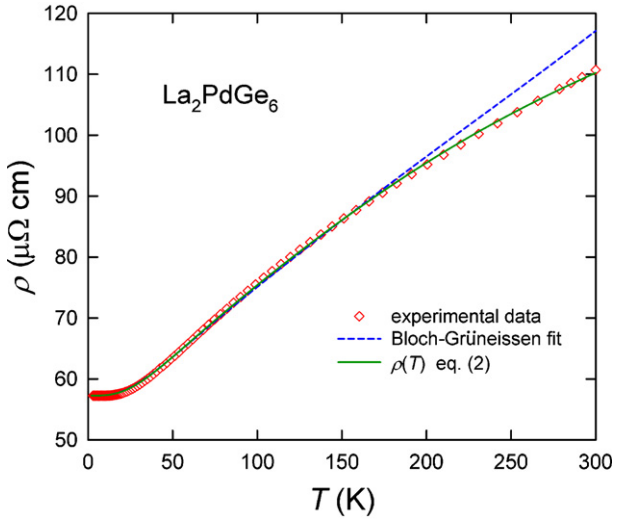

Fig. 3. Electrical resistivity vs. temperature of the polycrystalline La_2PdGe_6 (open diamonds). The solid line denotes the sum of ρ_0, the Bloch–Grüneissen and Mott *s–d* scattering contributions given by Eq. (2), whilst the dashed line presents the Bloch–Grüneissen term, ρ_{BG} (Eq. (1)).

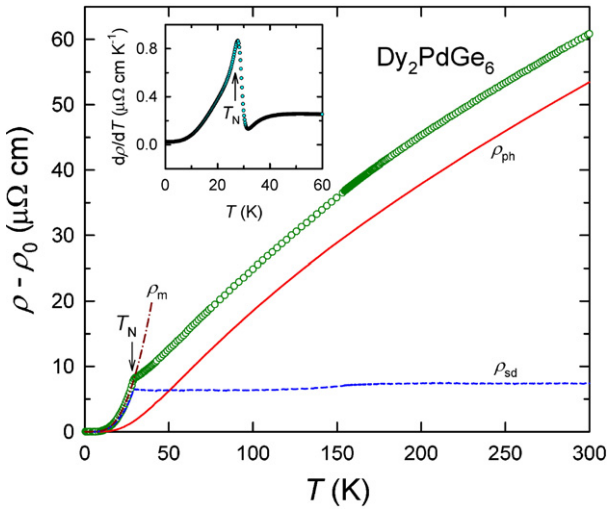

Fig. 4. Electrical resistivity vs. temperature after subtraction of residual resistivity, ρ_0 (=7.3 μΩ cm) for the polycrystalline Dy_2PdGe_6. The solid and dashed lines denote the phonon and spin-disorder contributions to the total resistivity, respectively, whereas ρ_m (dot-dashed line) displays the fit of low-*T* data to Andersen Eq. (3a) in Ref. [18]. Inset: the temperature derivative of the electrical resistivity, $d\rho(T)/dT$. T_N = 27.7 K.

about 80 K with an effective magnetic moment $\mu_{eff} = 10.62\mu_B$ and the paramagnetic Curie temperature $\theta_p = -18.6$ K. The former value is exactly as that expected for a theoretical value of a triple charged Dy^{3+} ion ($10.62\mu_B$). The negative value of θ_p is consistent with the AFM ordering as is just observed. Very similar magnetic parameters were also obtained previously for such isostructural compounds as Dy_2NiGe_6 [9] and Dy_2CuGe_6 [5]. Their Néel temperatures are 25 and 22 K, respectively.

Moreover, the free Dy^{3+} ion has the $^6H_{15/2}$ ground term, and $^6H_{13/2}$ first excited one at the distant energy of about 4620 K. The Landé factor for the sixteen fold degenerate ground-multiplet state, $g = 4/3$. A distinct effect of crystal electrical field (CEF) on the reciprocal susceptibility is seen below 80 K, where its downward deviation tendency takes place. In the lower inset of Fig. 1 the isothermal magnetization measured at $T = 1.9$ K is presented. As seen, the straight-line behaviour is only observed up to the critical field $B_{cr} = 3.5$ T. Above this field a metamagnetic transition occurs. Also for Dy_2NiGe_6 and Dy_2CuGe_6 the metamagnetic transitions at 3.2 T [8,9] and 1.5 T [5] were reported, respectively.

3.2. Electrical resistivity

Our first aim here is the presentation of the electrical properties of La_2PdGe_6 serving as the nonmagnetic isostructural reference compound that allows for subtracting from the total resistivity of Dy_2PdGe_6 approximately its phonon part. Thus Fig. 3 displays the temperature dependence of the resistivity $\rho(T) = \rho_0 + \rho_{ph}(T)$ of La_2PdGe_6 which behaves as a typical metallic material, but having rather a high value of the residual resistivity ρ_0 (57 μΩ cm).

This value however is lower than that reported for this La-based compound in Ref. [11] (74.5 μΩ cm). Also the slope of the reported overall $\rho(T)$ curve is higher than that of our curve. The obtained in this paper data $\rho_{ph}(T) = \rho(T) - \rho_0$ were then fitted to the generalized Bloch–Grüneissen relation $\rho_{BG}(T)$ given by Eq. (1) (dashed line in Fig. 2, see also e.g. for $ThCoGa_4$ [14]):

$$\rho_{BG}(T) = a\left(\frac{T}{\Theta_D^R}\right)^n \int_0^{\Theta/T} \frac{z^n dz}{(e^z - 1)(1 - e^{-z})}. \quad (1)$$

We used $n = 3$, which is more precise for various materials having a metallic character of resistivity, whereas the power $n = 5$ is more appropriate for the typical good metals, such as Cu, Ag, etc. The constant $a = 4R\Theta_D^R$, R is the coefficient of electron–phonon interaction and its value is of 0.05 μΩ cm K^{-1} for $\Theta_D^R = 195(2)$ K. Finally, we used the extended formula $\rho_{BGM}(T)$ given by Eq. (2) including the additional interband scattering *s–d* mechanism described by Mott [15] (the solid line in Fig. 3):

$$\rho_{BGM}(T) = \rho_0 + \rho_{BG}(T) + KT^3, \quad (2)$$

where ρ_0 is the residual resistivity due to lattice defects and impurities. All these terms together with Mott's term yield the similar *T*-variation as found for many other nonmagnetic intermetallic reference compounds, used as a phonon contribution (see for example Ref. [16]). Least-squares fitting of the whole BGM formula (2) to the experimental results in the whole temperature range yields the parameters as follows: $\rho_0 = 57$ μΩ cm and $K = -3.9 \times 10^{-7}$ μΩ cm K^{-3}. The same value Θ_D^R was reported for La_2CuGe_6 [10]. This parameter is usually considered as an approximation of the Debye temperature. Therefore one can assume that in both the La- and Th-based reference compounds the main scattering mechanism of charges is the phonon scattering.

In Fig. 4 there are plotted data of the overall temperature dependences of the electrical resistivity of Dy_2PdGe_6 (open circles) and La_2PdGe_6 (solid line) after subtracting their residual values ρ_0's. As seen, the corresponding $\rho(T) - \rho_0$ curves taken above about 30 K for both these germanides, are very similar to each other. Such a behaviour was also reported for other rare-earth intermetallics, like e.g. for the RIn_3 indides (R = Gd–Eb, Lu) [17a–c]. Hence, the solely magnetic part of Dy_2PdGe_6 in the paramagnetic region, being the spin-disorder contribution $\rho_{sd}(T)$, found by subtracting the $\rho_{ph}(T)$ dependence from the total resistivity of Dy_2PdGe_6 and reduced by ρ_0, is given in this figure by the dashed line. According to expectation, the ρ_{sd} behaviour in the whole paramagnetic region considered here is practically independent of temperature with a value of 7.5 μΩ cm. Surprisingly, there is difficult to see any distinct presence of the CEF effect as is also the case of the indides cited above [17c]. However, it is known that the latter interactions is considerably weaker for the intermetallics containing a heavy R_H element than those observed for the series with light R_L elements. In turn, the magnetic part $\rho_m(T)$ of Dy_2PdGe_6 below T_N exhibits a fast drop due to the ordering of the magnetic moments and varies accordingly with the relation given by Eq. (3a) for the electron–magnon

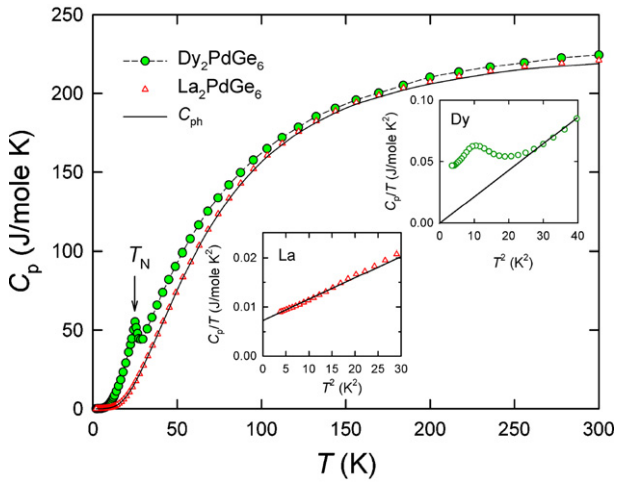

Fig. 5. Total specific heat C_p vs. T of Dy_2PdGe_6 (filled circles) and La_2PdGe_6 (open triangles). The solid line is an approximation of the phonon contribution, $C_{ph}(T)$. Insets: the C_p/T vs. T^2 dependences for both these compounds at the lowest temperatures measured.

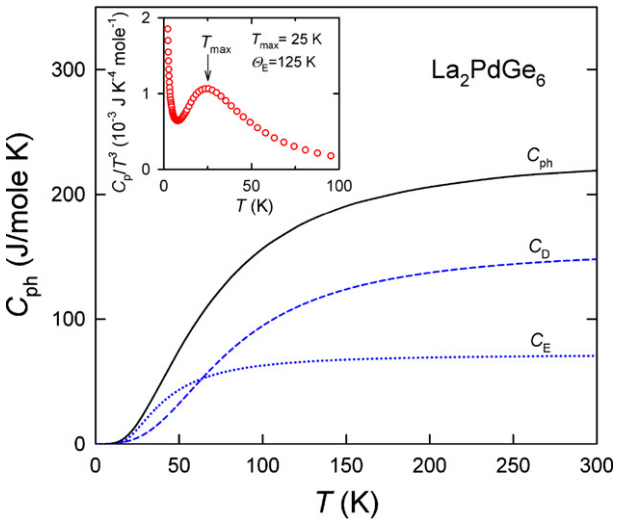

Fig. 6. The subtracted from the total specific heat of the La_2PdGe_6 phonon part (solid line) vs. T. The dashed line presents the Debye contribution C_D whilst the dotted line displays the Einstein contribution C_E. Their sum gives the solid line, i.e., both contribute into the phonon behaviour. The inset shows the C_p/T^3 vs. T plot which creates the Einstein temperature (see the text).

scattering process, reported by Andersen and Smith [18], completed by the first electron-electron scattering term:

$$\rho_m(T) = AT^2 + bT\left(1 + \frac{2T}{\Delta}\right)\exp\left(\frac{-\Delta}{T}\right) \quad (3a)$$

where $A = 7.4 \times 10^{-4}$ μΩ cm K^{-2}, $b = 0.568$ μΩ cm K^{-1} and $\Delta = 47$ K. The result of the fit is indicated as the dot-dashed line in Fig. 4. A quantitative description of the temperature dependence of the electrical resistivity also can be accomplished in terms of the model of Continentino [19], as given by Eq. (3b),

$$\rho_m(T) = c\Delta^{3/2}T^{1/2}\exp\left(-\frac{\Delta}{T}\right)\left[1 + \left(\frac{2}{3}\right)\left(\frac{T}{\Delta}\right) + \left(\frac{2}{5}\right)\left(\frac{T}{\Delta}\right)^2\right], \quad (3b)$$

where $c = 1.64 \times 10^{-2}$ μΩ cm K^{-2} and $\Delta = 57$ K (not shown in Fig. 4). The magnitudes of a gap in the magnon spectrum for this germanide, found by application of these two aforementioned models differ not so much from each other and are close to that reported by us in the case of Sm_2PdGe_6 (57 K) [13]. The goodness of the fits made above for $\rho_m(T)$ may be represented by the coefficient of determination, R^2, which is equal to 0.9998 and 0.9988 for Eqs. (3a) and (3b), respectively. These indicate that the former fit is a little bit better than the latter one. From the plot of the temperature derivative $d\rho(T)/dT$ vs. T (inset to Fig. 4) the evaluated value of T_N is a little higher than that inferred from the magnetic and thermal (see below) measurements.

3.3. Specific heat

Fig. 5 presents the total specific heats $C_p(T)$ for both Dy_2PdGe_6 (closed circles) and La_2PdGe_6 (open triangles). The latter has been used as a lattice phonon referrence $C_{ph}(T)$ of the former compound (see below). As the insets to this figure we present the C_p/T vs. T^2 curves taken for both these compounds. It appears, that at low temperatures due to the occurrence of a small maximum at about 3 K in the C_p/T_{Dy} vs. T^2 curve (right hand inset), likely due to some impurities in the sample, we were unable to find the Sommerfeld coefficient $\gamma_{Dy}(0)$ in a usual way. We could only extrapolate the C_p/T_{Dy} data to 0 K for temperatures above about 5.5 K from which one indicates $\gamma_{Dy}(0) \approx 0$. This value reported for example for the isostructural compound Ce_2PdGe_6, evaluated from experimental data below 0.45 K, is equal to 14 mJ/K^2 mole$_{Ce}$ [11]. However it was possible to determine $\gamma_{La}(0)$ and Θ_D^{La} from the low temperature C_p/T_{La} data plotted against T^2 (left hand inset), to be 3.6 mJ/K^2 mole$_{La}$ and 343 K, respectively. Taking the former value into account, the $C_{ph}(T)$ function has been evaluated after subtracting the electronic heat contribution $C_{el}(T)_{La} = 2 \times \gamma_{La}(0) \times T$ from the $C_p(T)$ data and plotted in Fig. 5 as the solid line.

Near room temperature C_p reaches asymptotically a value of about 225 J/K mole for both studied compounds that corresponds to the Dulong–Petit limit, i.e., $C_p = 3rR = 224.5$ J/K mole, for $r = 9$ atoms/molecule. R is a gas constant.

It should be noted that the earlier data for La_2PdGe_6, solely reported up to now [11], have been limited to the temperature range only below about 30 K. Therefore, we first will make a more detailed analysis of our phonon data measured up to 300 K. It is important to note that we could not get a satisfactory agreement between the fitting of one-phonon results to experiment. However, it was possible to using a two-phonon model. From the point of view of its components we have plotted in Fig. 6 the $C_{ph}(T)$ curve as a sum of the two specific heats originating from the Debye (C_D) and Einstain (C_E) models, calculated according to Eqs. (4).

Therefore, in Fig. 6 we show again the above extracted $C_{ph}(T)$ curve from Fig. 5, and in addition, we display in the inset to this figure the C_p/T^3 vs. T dependence at low temperatures. As seen this curve exhibits a maximum at $T_{max} = 25$ K indicating the presence of the optical modes in La_2PdGe_6, except for the obvious contribution of Debye modes. In the next step, we were able to deconvolute $C_{ph}(T)$ into the Debye, C_D, (dashed line) and Einstein, C_E, (dotted line) specific heat contributions, using Eqs. (4), which individually can be ascribed by the characteristic temperatures θ_D and θ_E, respectively. It turned out that the former corresponds to that found at low temperatures ($\theta_D = 343$ K) whilst the latter to that found from the well known dependence $\theta_E = 4.95\,T_{max}$ [20]. This temperature is then equal to $\theta_E \approx 125$ K. As seen from Fig. 6, only above $T \approx 70$ K the acoustic modes (C_D) start to dominate and become about two times greater than the optical ones (C_E) for $T > 250$ K. Eqs. (4) are as follows:

$$C_D = 9Nk_B\left(\frac{T}{\Theta_D}\right)^3\int_0^{\Theta_D/T}\frac{e^x x^4}{(e^x - 1)^2}dx,$$

$$C_E = 3Nk_B\frac{e^{\Theta_E/T}(\Theta_E/T)^2}{(e^{\Theta_E/T} - 1)^2}, \quad (4)$$

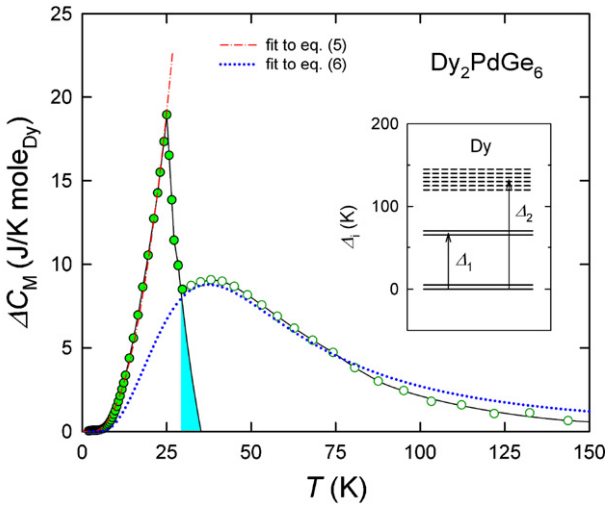

Fig. 7. Subtracted the magnetic C_m and Schottky C_{Sch} parts of the heat capacity ΔC_M (filled and open circles, respectively) vs. temperature. The dotted line presents the fit of Schottky contribution to Eq. (6). Inset: the energies Δ_1 and Δ_2 of the low lying CEF levels of Dy^{3+} ions.

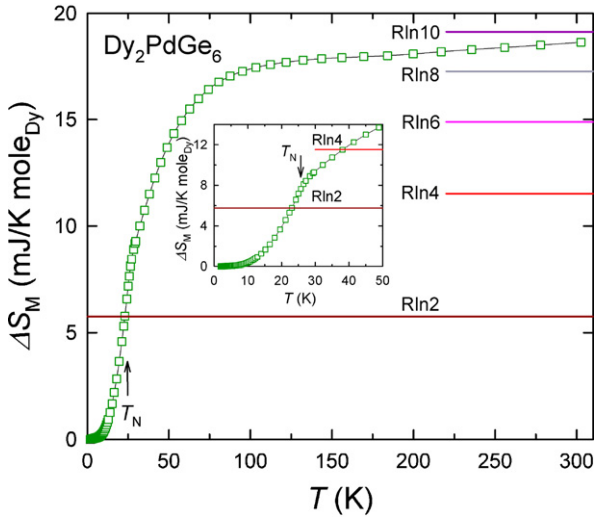

Fig. 8. The magnetic entropy ΔS_M vs. T. Inset shows this dependence at low-T on an enhanced temperature scale.

where N is the Avogadro number, k_B is the Boltzmann constant and $x = \hbar\omega_D/k_BT$.

The following formula $C_{ph}(T) = \rho_D C_D(\theta_D) + \rho_{Ei} C_E(\theta_E)$ was used to fit the phonon specific heat data from 2 to 300 K, where ρ_D and ρ_E are the vibraton modes for $r = 9$ atoms per molecule. For simplicity we used only one Einstein mode ($i = 1$). With nine atoms per molecule of La_2PdGe_6, there are in total $\rho_{ph} = 3 \times 9 = 27$ phonon modes: three acoustic and twenty four optical modes.

The magnetic part, ΔC_M, as a function of temperature up to 150 K is displayed in Fig. 7, where ΔC_M corresponds to two contributions: magnetic specific heat part C_m in the ordered state and Schottky part C_{Sch} in the paramagnetic state. By fitting the data to the above formula, the Debye and Einstain modes require $\rho_D = 18.36$ and $\rho_{E1} = 8.24$ numbers of oscillator strengths, respectively. This procedure is based on Ref. [21].

The $\Delta C_M(T)$ dependence was determined by subtracting from the total specific heat $C_p(T)$ of Dy_2PdGe_6 the phonon contribution approximated by our data of $C_p(T)_{La} - \gamma_{La}(0) \times T$, measured for the polycrystalline La_2PdGe_6. As shown in the left hand inset of Fig. 5, the Sommerfeld coefficient $\gamma_{La}(0) = 3.6\ mJ/mole_{La}\ K^2$.

The AFM transition is reflected by a sharp peak in $C_m(T)$ at $T_N = 25(1)$ K. Below the magnetic transition T_N, $C_m(T)$ can be well approximated by the formula (5):

$$C_m(T) = c\Delta^{7/2}T^{1/2}\ \exp^{-\Delta/T}\left[1 + \frac{39T}{20\Delta} + \frac{51}{32}\left(\frac{T}{\Delta}\right)^2\right], \qquad (5)$$

being appropriate for excitations of AFM spin waves with a gap Δ in the magnon spectrum [19]. The least squares fit of Eq. (5) to the experimental data taken just below T_N (shown in Fig. 7 by the dot-dashed curve) yields the following coefficients: $c = 4.62 \times 10^{-5}\ J/mole_{Dy}\ K^4$ and $\Delta = 18$ K. The latter value is much lower than those found from the electrical resistivity after applying Eqs. (3a) and (3b) (47 or 57 K).

Above T_N, the Schottky contribution C_{Sch} is formed by passing through a maximum at about $T_{max} = 35$ K. The total contribution ΔC_M, containing the magnetically ordered C_m and paramagnetic parts C_{Sch}, assuming that the electronic specific heat part C_{el} is zero, at temperatures up to 150 K is presented in Fig. 7. The shadow area indicates some short magnetic order described by the T^{-2} dependence. In turn, the dotted line presents the fit of the latter contribution to Eq. (6) where each part is proper for simplified three level system taken here schematically into account with the corresponding energy splitting by $E_i/k_B = \Delta_i$ (in K units):

$$C_{Sch}(T) = R\left[\frac{\sum_i g_i e^{-\Delta_i/T}\sum_i g_i\Delta_i^2 e^{-\Delta_i/T} - [\sum_i g_i\Delta_i e^{-\Delta_i/T}]^2}{T^2[\sum_i g_i e^{-\Delta_i/T}]^2}\right] \qquad (6)$$

where R is a gas constant, g_i is a degeneracy of the energy level and Δ_i ($i = 1$ and 2) is the energy difference (in units of temperature) between the two CEF levels, i.e. between the ground doublet and the first excited doublet (Δ_1) as well as between the former and the second excited levels taken here for simplicity as pseudo-sextet one (Δ_2). The schematic crystal field splitting for Dy^{3+} ions is shown in the inset of Fig. 7. The obtained values of Δ_1 and Δ_2 are about of 65 and 130 K, respectively. The fitting is quite good up to 75 K. However, at higher temperatures the calculated C_{Sch}^{th} dependence becomes slightly larger than the experimental curve C_{Sch}^{exp} but within a range of the expected experimental error, typical of this kind of fittings. The scheme shown in the inset of Fig. 7 presents an oversimplification of the problem and should be treated only as a demonstrative case. In turn, Fig. 8 presents the magnetic entropy ΔS_M found by the integration of the $(\Delta C_M/T)dT$ function from 0 to 300 K.

This may indicate that the magnetic ground state is a Kramers doublet. At higher temperatures, one expects a thermal population of the remaining doublets inferring from Hund's rules of the $^6H_{15/2}$ ground multiplet. According to the crystal field scheme, given in the inset to Fig. 7, the amount of entropy close to RT is equal to about $R \ln 10$. Hence to attain the full Hund's rule value of $R \ln 16$, one needs higher temperatures than RT. For the sake of comparison, we mention here that the total splitting energy of $^6H_{15/2}$ multiplet of Dy^{3+} in DyF_3, crystallizing in the orthorhombic space group *Pnma*, is even as high as about 700 K [22]. Any more detailed treatment of such topics as above requires an adequate different kind of measurements made on single-crystalline samples.

3.4. Thermoelectric power

The thermoelectric power (TEP) of both compounds La_2PdGe_6 and Dy_2PdGe_6 is shown in Fig. 9. This quantity for La_2PdGe_6 is negative in the whole measured temperature range with almost linear dependence above 150 K. Contrastingly, $S(T)$ for Dy_2PdGe_6 is positive, excluding a short temperature range below about T_N, where $S(T)$ changes its sign and then passes through a small negative

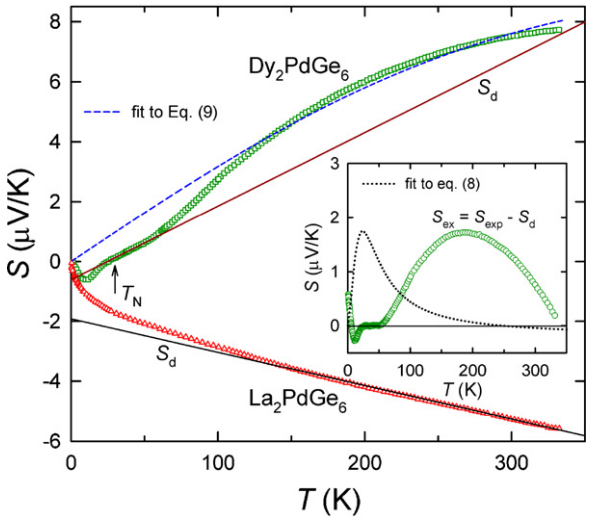

Fig. 9. Thermoelectric power vs. temperature for Dy_2PdGe_6 (squares) and La_2PdGe_6 (triangles) measured on the polycrystalline samples. The solid lines present the expected diffusion terms S_d^{exp} for La- and Dy-ternaries. The dashed line indicates $S(T)$ calculated by using Eq. (9). The inset displays the diffusion, S_d (taken here as zero line), and excess S_{ex} parts (open circles). The dotted line represents the expected crystal field S_{CF} contributions to the total thermoelectric power, according to the scheme shown in the inset of Fig. 7.

minimum at $T_{min} = 10.7$ K reaching a value $S_{min} = -0.6$ μV/K. Below T_{min}, as expected, $S(T)$ goes to zero at $T = 0$ K. It should be noted that negative values of S are involved with the temperature range of magnetic ordering. At temperatures between T_N and 70 K there is a linear segment in $S(T)$ behaviour, after which a wide hump in the temperature dependence of the thermoelectric power occurs up to about 350 K. The solid straight line drawn at low-T through the experimental points of Dy_2PdGe_6 at temperatures mentioned above may denote the expected diffusion term of thermoelectric power $S_d^{exp} = aT$, which usually varies linearly with temperature according to the Mott relation [23]:

$$S_d(T) = \frac{\pi^2 k_B^2 T}{3eE_F}, \tag{7}$$

where e is the charge of an electron and E_F is the Fermi energy.

Next, we extract the hump mentioned above by plotting in the inset to Fig. 9 the difference $S(T) - aT$ against temperature. Furthermore, by the dotted curve we have marked in this inset the expected crystal field contribution to the thermoelectric power, according to the energy scheme found from the Schottky fitting procedure by applying Eq. (8):

$$S_{CF} = \text{constant} \times F\left(\frac{T}{\Delta_i}\right) \tag{8}$$

where the function $F(T/\Delta_i)$, is a universal function with a maximum at $T_{max} \approx 0.3\Delta_i$ for a single separation Δ_i of the CEF levels [24]. As apparent from this figure, this kind contribution to the thermoelectric power practically does not exist. It leads to a conclusion that the wide hump may be analysed using a phenomenological model of conduction electrons scattered by a narrow band of Lorentzian form located near the Fermi energy [25]. Within the so-called two-band model the Seebeck coefficient is thus given by Eq. (9):

$$S(T) = \frac{AT}{(B^2 + T^2)}, \quad A = \frac{2\Delta}{|e|}, \quad B^2 = \frac{3(\Delta^2 + \Gamma^2)}{\pi^2 k_B^2}, \tag{9}$$

where Δ is the position of the narrow band relative to E_F. Γ is the bandwidth. As a result, the dashed curve in the figure yields a satisfactory description of the hump (at least at higher temperatures) observed in the thermoelectric power of Dy_2PdGe_6.

A similar behaviour of $S(T)$ exhibits a number of rare earth and uranium intermetallics, as e.g. ErPdBi [26] or CePdSb, UPt_2In, UNi_4B and $U(Ni:Pd)_2Al_3$ [27] but particularly for UPd_2Sb [28].

4. Conclusions

We have measured and analysed the temperature dependences of magnetic susceptibility, electrical resistivity, specific heat and thermoelectric power for isostructural Dy_2PdGe_6 and La_2PdGe_6. The latter nonmagnetic compound was specially synthesized in order to eliminate the phonon contributions and this way to extract the magnetic characteristics of Dy_2PdGe_6.

This Dy-germanide is an antiferromagnet with $T_N = 25(1)$ K as those studied previously also by us such ternaries containing Ce and Sm. If La_2PdGe_6 is a typical metal, its Dy-counterpart exhibits a semimetallic-like electrical conductivity. The behaviour of the latter may be described by assuming the presence of a narrow gap in its magnon spectrum in the AFM state.

We have also performed a broader analysis of the phonon behaviour of La_2PdGe_6. We found that only combining acoustic with optical phonons can give any satisfactory agreement between the fitting results and experimental data. Taking into account the phonon contribution to the total specific heat of Dy_2PdGe_6 one has allowed to separate the magnetic peak caused by an antiferromagnetic order and Schottky anomaly caused by CEF effect. Analysing the latter, we have made fitting to a preliminary CEF scheme of lower energy levels which yield the magnetic entropy of $R \ln 10$ at RT with the lowest Kramers doublet as the ground state. Unfortunately, no CEF effect has been seen in the temperature dependences of the magnetic part of the electrical resistivity and thermoelectric power. In the case of the latter measurements, we have revealed the positive sign of Seebeck coefficient of Dy_2PdGe_6 in the paramagnetic region of temperatures indicating that the holes are dominant carriers in this region. On the other hand, $S(T)$ in the ordered state of Dy- and in the whole temperature range of La-germanides is negative pointing to the domination of electron-type carriers. Finally, we were able to fit the $S(T)$ data to the sum of the two contributions, a linear diffusion part S_d and a convex two-band conductor model part S_{ex} by assuming a single Lorentzian 4f band, appropriate for an existence of some hybridization between 4f and conduction electrons.

Acknowledgement

This work is supported by Russian Foundation for basic Research (RFII, grant number 11-03-01191).

References

[1] O. Sologub, K. Hiebl, P. Rogl, O.I. Bodak, J. Alloys Compd. 227 (1995) 37.
[2] M.B. Konyk, P.S. Salamakha, O.I. Bodak, V.K. Pecharsky, Kristallografia 33 (1988) 838.
[3] M.L. Fornasini, P. Manfrinetti, A. Palenzona, Z. Kristallogr. NCS 217 (2002) 173.
[4] M.B. Konyk, L.P. Romaka, Yu.K. Gorelenko, O.I. Bodak, J. Alloys Compd. 311 (2000) 120.
[5] D. Kaczorowski, M. Konyk, A. Szytuła, L. Romaka, O. Bodak, Solid State Sci. 10 (2008) 1891.
[6] K. Shigetoh, F. Hirata, M.A. Avila, T. Takabatake, J. Alloys Compd. 403 (2005) 15.
[7] A. Szytuła, M. Konyk, B. Penc, A. Winiarski, Acta Phys. Pol. 113 (2008) 1205.
[8] M. Konyk, L. Romaka, Yu. Gorelenko, O.I. Bodak, Visnyk Lviv Univ. Ser. Khim. 45 (2004) 105.
[9] M. Konyk, L. Romaka, D. Gignoux, D. Fruchart, O.I. Bodak, Yu Gorelenko, J. Alloys Compd. 398 (2005) 8.
[10] M. Konyk, B. Kuzhel, Yu Stadnyk, Yu Gorelenko, Ya Mudryk, A. Waskiv, J. Alloys Compd. 459 (2008) 18.
[11] Y.T. Fan, W.H. Lee, Y.Y. Chen, Phys. Rev. B 69 (2004) 132401.
[12] A.M. Strydom, A.V. Gribanov, Yu.D. Seropegin, R. Wawryk, R. Troć, J. Magn. Magn. Mater. 283 (2004) 181.
[13] R. Troć, R. Wawryk, K. Gofryk, A.V. Gribanov, Yu.D. Seropegin, J. Phys.: Condens. Matter 23 (2011) 146001.

[14] R. Wawryk, J. Stępień-Damm, Z. Henkie, T. Cichorek, F. Steglich, J. Phys.: Condens. Matter 16 (2004) 5427.
[15] N.F. Mott, Proc. R. Soc. 156 (1936) 368.
[16] Z. Kletowski, R. Fabrowski, P. Sławiński, Z. Henkie, J. Magn. Magn. Mater. 166 (1997) 361.
[17] (a) Z. Kletowski, P. Sławiński, Solid State Commun. 76 (1990) 867;
(b) Z. Kletowski, P. Sławiński, A. Czopnik, Solid State Commun. 80 (1991) 981;
(c) Z. Kletowski, Solid State Commun. 81 (1992) 297.
[18] N.H. Andersen, N.H. Smith, Phys. Rev. B 19 (1979) 384.
[19] M.A. Continentino, S.N. de Medeiros, M.T.D. Orlando, M.B. Fontes, E.M. Baggio-Saitovitch, Phys. Rev. B 64 (2001) 012404.
[20] A. Junod, T. Jarlborg, J. Muller, Phys. Rev. B 27 (1983) 1568.
[21] A.P. Ramirez, G.R. Kowach, Phys. Rev. Lett. 80 (1998) 4903.
[22] A.V. Savinkov, S.L. Korableva, A.A. Rodionov, I.N. Kurkin, B.Z. Malkin, M.S. Tagirov, H. Suzuki, K. Matsumoto, S. Abe, J. Phys.: Condens. Matter 20 (2008) 485220.
[23] R.D. Bernard, Thermoelectricity in Metals and Alloys, Taylor and Francis Ltd, London, 1972.
[24] P. Fulde, I. Peschel, Adv. Phys. 21 (1972) 1.
[25] U. Gottwick, K. Gloos, S. Horn, F. Steglich, N. Grewe, J. Magn. Magn. Mater. 47–48 (1985) 536.
[26] D. Kaczorowski, K. Gofryk, T. Plackowski, A. Leithe-Jasper, Yu. Grin, J. Magn. Magn. Mater. 290–291 (2005) 573.
[27] Y. Bando, T. Suemitsu, K. Takagi, H. Tokushima, Y. Echizen, K. Katoh, K. Umeo, Y. Maeda, T. Takabatake, J. Alloys Compd. 313 (2000) 1.
[28] K. Gofryk, D. Kaczorowski, A. Czopnik, Solid State Commun. 133 (2005) 625.